Desmin Filaments Studied by Quasi-Elastic Light Scattering

Melanie Hohenadl,* Tobias Storz,* Hulda Kirpal,* Klaus Kroy,# and Rudolf Merkel*
*Lehrstuhl für Biophysik, E22 and #Lehrstuhl für theoretische Physik, T34, Technische Universität München, James-Franck-Str. 1, D-85748 Garching, Germany

ABSTRACT We studied polymers of desmin, a muscle-specific type III intermediate filament protein, using quasi-elastic light scattering. Desmin was purified from chicken gizzard. Polymerization was induced either by 2 mM $MgCl_2$ or 150 mM NaCl. The polymer solutions were in the semidilute regime. We concluded that the persistence length of the filaments is between 0.1 and 1 μm. In all cases, we found a hydrodynamic diameter of desmin filaments of 16–18 nm. The filament dynamics exhibits a characteristic frequency in the sense that correlation functions measured on one sample but at different scattering vectors collapse onto a single master curve when time is normalized by the experimentally determined initial decay rate.

INTRODUCTION

The cytoskeleton is a central and vital part of eukaryotic cells. It consists of a network of partially interconnected polymers. This extended network controls the mechanical properties of animal cells, serves as "tracks" for intracellular transport, and plays a prominent role in cell motility (Alberts et al., 1994). The cytoskeleton is composed of three different filament types (i.e., actin filaments, microtubules, and intermediate filaments) and a plethora of cross-linking and regulating proteins (Houseweart and Cleveland, 1998). Whereas our knowledge of the properties of actin filaments and microtubules is fairly advanced, much less is known about the function and properties of intermediate filaments (IFs). It appears that IFs are vital for cell function and integrity under mechanical stress.

In polymers formed by IF proteins, the basic monomeric unit is itself a macromolecule, in the case of desmin, with a molecular weight of 53,000 (Geisler and Weber, 1980). This results in polymers of very large size: about 12 nm in diameter and several micrometer in length. These polymers are inhomogeneous because they show a certain variation in thickness (Heins and Aebi, 1994). In living cells, it was shown that labeled keratins (another member of the IF family) are incorporated along the whole length of already existing filaments (Miller et al., 1991). Polymers of IF proteins were, up to now, mostly characterized by methods from cell and molecular biology. In this study, we attempt a physical characterization. Two key parameters for the description of polymers are the diameter and the persistence length. Here we investigated both parameters by quasi-elastic light scattering.

IF proteins form a very heterogeneous family of proteins (Goldman et al., 1990). To date, six different classes of IF proteins are distinguished according to common motifs in the amino acid sequence (Quinlan et al., 1995). In this work, we report in vitro experiments on desmin, a muscle-specific type III IF protein (Lazarides, 1980; Fuchs and Weber, 1994). In mature skeletal muscle, desmin filaments interconnect myofibrils at their Z disc levels to keep them in register within the muscle fiber (Lazarides, 1980; Small et al., 1992; Fuchs and Weber, 1994). In view of this important function, it is not surprising that genetically engineered mice lacking desmin exhibit severe disruption of muscle architecture and muscle degeneration (Milner et al., 1996). The most important property of IF proteins is their ability to self-organize into filaments under the appropriate buffer conditions (Lazarides, 1980; Stewart, 1990). In living cells, filament formation is controlled through phosphorylation (O'Connor et al., 1979; Inagaki et al., 1987) and possibly also ADP-ribosylation (Zhou et al., 1996). In vitro filament formation can be induced by changing the buffer conditions. Desmin is soluble only under highly unphysiological conditions like 8 M urea or at basic pH and low ionic strength, whereas reduction of the pH to physiological values combined with an increase of the buffer's ionic strength results in polymerization (Huiatt et al., 1980; Chou et al., 1990). At the present time, the polymerization mechanism is not well understood. Recent studies on vimentin, an IF protein closely related to desmin, suggested that polymerization is a two-step process. First, building blocks (tetra- or octamers) form, which subsequently fuse into elongating filaments that grow to lengths of many micrometers (Herrmann et al., 1996; Herrmann and Aebi, 1998). Rheological experiments on vimentin gels indicated that IF protein networks exhibit highly interesting mechanical properties on a macroscopic scale, i.e., strain hardening and a high resistance against rupture (Janmey et al., 1991). It is not obvious whether these characteristics stem from single filament properties or the interactions between filaments. In this work, we used dynamic light scattering to probe the mechanical properties of desmin polymers on a micrometer length scale. Simultaneous with our work, Janmey and coworkers were using the same technique to study vimentin, another class III IF protein, and came to comparable conclusions.

Received for publication 30 November 1998 and in final form 4 June 1999.
Address reprint requests to Rudolf Merkel, Lehrstuhl für Biophysik, E22, Technische Universität München, James-Franck-Str. 1, D-85748 Garching, Germany. Tel: +49-89-2891-2480; Fax.: +49-89-2891-2469; E-mail: rmerkel@physik.tu-muenchen.de.
© 1999 by the Biophysical Society
0006-3495/99/10/2199/11 $2.00

In recent years, it was shown that dynamic light scattering is a valuable tool for the study of biopolymers. The underlying reason for this success is the enormous size of these polymers. In our experiments, we studied networks with a mesh size of about 1 μm formed by 16-nm-thick polymers exhibiting a persisting length below 1 μm. All characteristic length scales are on the order of the wavelength of visible light, which makes light scattering an appropriate technique to study these networks. For most biopolymers, neither thickness nor stiffness may be neglected on the length scale of light-scattering experiments. On one hand, this complicates the interpretation of the measurements considerably; on the other hand it enables us to extract characteristic quantities like the persistence length or the hydrodynamic diameter of biopolymers from these measurements. This intriguing situation stimulated theoretical and experimental work that resulted in a coherent picture for dilute and semidilute solutions of weakly bending rods (Maeda and Fujime, 1984, 1985; Fujime et al., 1984; Janmey et al., 1986; Farge and Maggs, 1993; Drögemeier et al., 1994; Kroy and Frey, 1996; Götter et al., 1996). Long polymers exhibiting persistence lengths on the order of the scattering length pose a difficult theoretical problem. Unlike the aforementioned cases, no entirely satisfactory approach is available. The situation is nicely discussed in the work of Harnau et al. (1995). For the case of very flexible polymers, the well established Rouse or Zimm model (Zimm, 1956; de Gennes, 1967; Dubois-Violette and de Gennes, 1967; Akcasu et al., 1980) may be used to interpret the results. Interestingly, we found in our experiments on desmin filaments that the initial decay could be consistently evaluated using the theory for weakly bending rods (Kroy and Frey, 1996; Arcovito et al., 1997), whereas the rest of the decay was intermediate between the models of Rouse and Zimm.

THEORETICAL CONSIDERATIONS

Light propagating in transparent media is scattered by spatial fluctuations of the dielectric constant (Berne and Pecora, 1976). A fraction of this scattered light is frequency shifted due to the Doppler effect. It therefore contains information about the sample dynamics. Extraction of this information is the objective of dynamic light scattering experiments (Berne and Pecora, 1976; Chu, 1991). Our experiments were performed in the homodyne mode, sometimes also called self-beating mode. In this mode, the measured quantity is the correlation function of the intensity scattered at a defined scattering vector, $g^{(2)}(\tau)$. The field correlation function $g^{(1)}$ is the central quantity in most theoretical approaches to polymer dynamics. It is connected with the intensity correlation function by the Siegert relation (Chu, 1991)

$$g^{(2)}(\tau) = 1 + |g^{(1)}(\tau)|^2. \tag{1}$$

The scattering amplitude and dynamics depend on the scattering wave vector $\vec{q}$ (Berne and Pecora, 1976), the magnitude of which is given by

$$q = \frac{4\pi n}{\lambda} \sin(\theta/2). \tag{2}$$

Here, n denotes the refractive index of the medium, θ the angle between the incoming laser beam and the direction of the scattered light (i.e., the direction of observation), and λ the wavelength of the light in vacuum, which is only very minutely changed by quasi-elastic scattering events. In dilute and semidilute solutions, the probability of finding more than one polymer in a volume of $(1/q)^3$ is very small, therefore the correlation functions are entirely determined by contributions from single polymers. The field correlation function for dilute and semidilute polymer solutions was calculated for different models, two of which we will briefly present below.

The standard models for polymer dynamics are the Rouse and Zimm models (Zimm, 1956; Doi and Edwards, 1986). In these models, the polymer is represented by a series of beads interconnected by springs and is assumed to obey Gaussian statistics on all length scales. In the Zimm model, hydrodynamic interaction between different beads is accounted for in an approximate way, whereas this effect is entirely neglected in the Rouse model.

Within these models, the field correlation function was calculated analytically (de Gennes, 1967; Dubois-Violette and de Gennes, 1967; Akcasu et al., 1980). The resulting equation for the Rouse model is

$$\begin{aligned} g^{(1)}(\tau) &= \int_0^\infty \mathrm{d}u \exp\left[-u - (\Gamma_q t)^{1/2} h\left(\frac{u}{(\Gamma_q t)^{1/2}}\right)\right] \\ h(z) &= 2\Big/\pi \int_0^\infty \mathrm{d}x \frac{\cos(xz)}{x^2}\left[1 - \exp(-x^2)\right] \\ \Gamma_q &= \frac{k_B T}{12\xi_0} q^4 a^2. \end{aligned} \tag{3}$$

Here, k_B denotes Boltzmann's constant, ξ_0 the drag on a single bead, and a the radius of the bead. For the Zimm model, the result is

$$\begin{aligned} g^{(1)}(\tau) &= \int_0^\infty \mathrm{d}u \exp\left[-u - (\Gamma_q t)^{2/3} h\left(\frac{u}{(\Gamma_q t)^{2/3}}\right)\right] \\ h(z) &= 2\Big/\pi \int_0^\infty \mathrm{d}x \frac{\cos(xz)}{x^2}\left[1 - \exp\left(-\frac{x^{2/3}}{\sqrt{2}}\right)\right] \\ \Gamma_q &= \frac{k_B T}{6\pi\eta_S} q^3 \\ g^{(1)}(t) &\approx \exp(-\alpha\Gamma_q t) \quad \text{for} \quad \Gamma_q t \ll 1. \end{aligned} \tag{4}$$

Here, η_s denotes the solvent viscosity, and α is a correction factor that is exactly one for the calculation of Dubois-

Violette and de Gennes, who used a preaveraged Oseen tensor and Θ conditions. The initial decay was also calculated omitting these simplifying assumptions. In good solvent, α was found to be 1.34 (Akcasu et al., 1980). Preaveraging the Oseen tensor could also be omitted; in which case α values of 1.18 for Θ conditions (Akcasu et al., 1980) and 1.49 for good solvent conditions were found (Benmouna and Akcasu, 1980). It is very important to realize that the field correlation function is a scaling function of one single variable $\Gamma_q t$ only. In other words, the entire decay of the correlation function is characterized by a unique characteristic frequency Γ_q that may be determined from the initial decay. Because this model does not take account of the local structure of the polymer chain, it is not surprising that it fails to describe all properties of desmin filaments.

To deal explicitly with the inherent stiffness of the polymers, different models must be used. The most successful one has been proposed by Kratky and Porod (1949) and has been used later to calculate the decay of the dynamic structure factor of semiflexible polymers (Maeda and Fujime, 1984; Kroy and Frey, 1996, 1998). Again, simple expressions could only be derived in the long- and short-time limits. The initial decay is given by (Kroy and Frey, 1996)

$$\begin{aligned} g^{(1)}(t) &= \exp\left(-\frac{2}{3\pi}\gamma_i t\right) \quad \text{for} \quad t \ll \tau_q \\ \tau_q &= \frac{\zeta_\perp}{\kappa q^4} \\ \gamma_i &= \frac{k_B T}{\zeta_\perp} q^3. \end{aligned} \tag{5}$$

In these equations, κ is the bending stiffness of the polymer and $\zeta_\perp$ the friction coefficient. In this model, the friction coefficient is weakly dependent on the magnitude of the scattering vector. For dilute solutions, the friction coefficient has a simple form (Kroy and Frey, 1996)

$$\zeta_\perp = \frac{4\pi\eta_s}{5/6 - \ln(q a_h)}. \tag{6}$$

Here η_s denotes the solvent viscosity and a_h the hydrodynamic diameter of the polymer.

Because the mesh size of the network, ξ_m, is relatively large, i.e., $q\xi_m > 1$, one expects the effects of steric and hydrodynamic interactions between the filaments on the dynamic structure factor to be small. However, because the concentrations of our solutions were, in some cases, close to this threshold, we wanted to check the validity of the expressions for the dilute limit. The importance of hydrodynamic interactions of a test filament with the surrounding filaments may be approximately estimated within the theory of hydrodynamic screening (Doi and Edwards, 1986). The resulting expression for the friction coefficient in the presence of hydrodynamic screening is (Kroy and Frey, 1996)

$$\begin{aligned} \zeta_\perp^{-1} = [&28 - 30\ln(q a_h) + 6q^{-2}\xi_h^{-2} \\ &-6q^{-3}\xi_h^{-3}\arctan(q\xi_h) - 30q^{-1}\xi_h^{-1}\arctan(q\xi_h) \\ &-3(q^2\xi_h^2 + 5)\ln(1 + q^{-2}\xi_h^{-2})]/(180\pi^2\eta_s). \end{aligned} \tag{7}$$

Here, ξ_h denotes the hydrodynamic screening length. According to the theory of Edwards and Muthukumar (1984), the hydrodynamic screening length in a solution of rods behaves essentially like the mesh size as a function of concentration. As a plausible assumption, we set $\xi_h = \xi_m$ in the expression for the initial decay rate in the presence of hydrodynamic screening. The mesh size was estimated using a mass per length of desmin filaments of 52 kDa/nm (Herrmann et al., 1997) and the assumption that we may approximate the random network by a square lattice for this purpose. In the Results section, we will show that, for our experiments, Eq. 7 yielded results that deviated little from the results of Eq. 6, i.e., the effect of hydrodynamic screening was indeed weak.

On a longer time scale a stretched exponential tail of the structure factor was predicted (Farge and Maggs, 1993; Kroy and Frey, 1996),

$$\begin{aligned} g^{(1)}(t) &= \exp\left[-\frac{\Gamma(1/4)}{3\pi}(\gamma_s t)^{3/4}\right] \quad t \gg \tau_q \\ \gamma_s &= \frac{k_B T q^{8/3}}{\zeta_\perp l_p^{1/3}}. \end{aligned} \tag{8}$$

Here, Γ denotes the gamma function and l_p the persistence length of the polymer, which is given by its bending stiffness via $l_p = \kappa/(k_B T)$. All other symbols were defined above for Eq. 5. However, this stretched exponential tail is only expected if the persistence length is much larger than the scattering length $1/q$.

More precisely, the time decay of the dynamic structure factor is, first of all, determined by the time γ_s^{-1} in the sense that $g^{(1)}(t) \sim 1$ for $\gamma_s t \ll 1$ and $g^{(1)}(t) \ll 1$ for $\gamma_s t \gg 1$. For a solution that is sufficiently dilute so that interactions are scarce on the time scale γ_s^{-1}, one can further distinguish two regimes in the decay of $g^{(1)}(t)$: 1) the initial decay regime described by Eq. 5 for $t \ll \tau_q$, and 2) the stretched exponential regime described by Eq. 8 for $t \gg \tau_q$. In contrast to the Rouse–Zimm model, how much each of the two regimes contributes to the total decay of $g^{(1)}(t)$ depends on system parameters (i.e., on the ratio $q l_p$ of persistence length to scattering wavelength). For $q l_p \gg 1$, which was assumed for the derivation of Eqs. 5–8, the relations $\tau_q \ll \gamma_i^{-1} \ll \gamma_s^{-1}$ hold, and the decay is mainly due to the stretched exponential tail. In the limit $q l_p \to 1$, the characteristic time scales γ_i^{-1}, γ_s^{-1}, and τ_q become identical. If we assume that the description remains valid (at least qualitatively) in this limit, we can immediately draw two important conclusions. First, the scattering functions of sufficiently flexible polymers should collapse if rescaled by γ_i, because γ_i is the only characteristic time scale left; whereas data

collapse cannot be achieved for somewhat stiffer molecules, where the different time scales are separated. (We note that data collapse can again be achieved for very stiff polymers, i.e., if τ_q is small compared with the shortest measurement time, and time is rescaled by γ_s.) Second, with increasing flexibility, the tail regime is shifted to longer times (it occurs for $t \gg \tau_q \sim \gamma_s^{-1}$, where $g^{(1)}(t) \ll 1$ already) so that the scaling function approaches the simple exponential of Eq. 5.

MATERIALS AND METHODS

Protein purification

Our method for desmin purification from chicken gizzard is a modification of published procedures (Geisler and Weber, 1980; Huiatt et al., 1980). The basic steps of the procedure are: 1) homogenization of the tissue and lysis of the cells; 2) washing the homogenized material with KCl and KJ buffers, which results in enrichment of desmin and, at the same time, partial removal of actin, myosin, tropomyosin, and some other proteins; 3) solubilization of desmin in urea; and 4) final purification by ion-exchange chromatography. The first steps were performed as described or proposed by Geisler and Weber, the last step was modified.

All steps were performed at 4°C. Chickens were slaughtered and disemboweled by a local farmer. Gizzards were frozen immediately after evisceration and stored at −70°C. Gizzards were thawed, cleaned, cut into small pieces, and then homogenized in buffer A (see below) using a blender. Typically, 50 g of cleaned gizzard were used. The homogenized material was suspended in 1 L buffer A, stirred for one hour and subsequently centrifuged at 8300 × *g* for 20 min. The resulting pellet was resuspended in 1 L buffer B, homogenized for a few seconds, stirred 10 min, and then centrifuged for 15 min. Washing with buffer B was repeated twice. After the last centrifugation, the pellet was suspended in 1 L buffer C and gently stirred overnight. This suspension was then centrifuged for 20 min. Washing with buffer C was performed three times. For the second washing, the suspension was stirred for 1.5 h, otherwise the procedure was executed as described above. The resulting pellet was suspended in 200 mL buffer D, stirred overnight and centrifuged for 30 min. Desmin was contained in the supernatant, which was carefully decanted. This solution was dialyzed twice against 1 L buffer E. A HiTrap cation exchange high-performance column (5 mL volume, Pharmacia, Uppsala, Sweden) was equilibrated with 50 mL buffer E, flushed with 25 mL of the same buffer with 1 M NaCl added, and again eluted with 100 mL buffer E. The column was connected to a UV monitor (Pharmacia). Protein solution, 30 mL, was applied to the column, and, subsequently, buffer E was passed through until the base line-level was reached again. For this to happen, approximately 25 mL buffer were necessary. Desmin was eluted by a linear salt gradient (0–0.4 M NaCl) and collected in fractions. This procedure was repeated with the desmin fractions that were previously dialyzed against buffer E, but, this second time, a flatter NaCl gradient was used. This last chromatographic step resulted in an efficient separation of desmin from other proteins. The final concentrations of desmin were approximately 0.4–1.0 mg/mL. Protein purity was checked by sodium dodecylsulfate gel electrophoresis. This purification procedure resulted in desmin that was at least 95% pure. Tests using gel electrophoresis showed that desmin could be stored at least 6 months at 4°C in buffer E with an addition of about 0.2 M NaCl without any changes in relative molecular weight or the appearance of additional bands on the gel.

Buffers

Buffer A: 0.6 M KCl, 40 mM imidazole (1,3-diaza-2,4-cyclopentadiene), 1 mM ethylene glycol-*bis*(β-aminoethyl ether)*N*,*N*,*N*′,*N*′-tetraacetic acid (EGTA), 0.5 mM DL-dithiothreitol (DTT), 0.5% t-octylphenoxypolyethoxyethanol (triton X-100), pH 6.9.

Buffer B: Buffer A without triton X-100.

Buffer C: 0.6 M KJ, 10 mM imidazole, 1 mM EGTA, 0.5 mM DTT, 0.2 mM adenosine 5′-triphosphate (ATP), 0.5% triton X-100, pH 6.9.

Buffer D: 8 M urea, 10 mM tris[hydroxymethyl]aminomethane acetate (TRIS HAc), 1 mM ethylenediaminetetraacetic acid (EDTA), 0.5 mM DTT, pH 7.0.

Buffer E: 6 M urea, 20 mM TRIS HAc, 1 mM EGTA, 0.5 mM DTT, pH 7.0.

KCl, KJ, imidazole, urea, and NaCl were bought from Merck (Darmstadt, Germany), EGTA, EDTA, triton X-100, DTT, and TRIS HAc from Sigma (Deisenhofen, Germany), and ATP from Serva (Heidelberg, Germany). Urea solutions were prepared from a stock solution (6 M urea) that had just been passed through a column of AG 501-X8(D) mixed bed ion exchange resin (BioRad, Munich, Germany) to remove cyanate and other ionic contaminations. Urea solutions were prepared freshly as needed and stored at 4°C to minimize cyanate formation.

Sample preparation and electron microscopy

Our procedures for sample preparation are based on the report by Chou et al. (1990). The basic steps are removal of denaturing urea, separation of dust and debris, and polymerization of desmin to filaments.

After purification, the samples were stored in 6 M urea, which was removed by extensive dialysis. (Three times 2 hr against 1 L TRIS, 10 mM, pH 8.5 [Sigma] followed by again three times 2 hr against 1 L sodium bicarbonate, 1 mM, pH 8 [Merck]. The second of the latter dialysis steps was sometimes performed overnight.) Debris was removed by 30 min centrifugation at 110,000 × *g*. Dialysis and centrifugation were performed at 4°C. Within half an hour after centrifugation, protein solutions were filtrated directly into freshly cleaned cylindrical quartz cuvettes (10 mm outer diameter, Hellma, Müllheim, Germany) using a 0.22-μm pore size filter (Millex GV4, Millipore, Bedford, MA). Filtration was done in a laminar flow hood (Beer Technik GmbH, Munich, Germany). The cuvettes had been cleaned with freshly distilled acetone in a dedicated cuvette cleaning and distillation glass apparatus (Küvettenspüler Mainz 70, Fischer Labortechnik, Frankfurt/Main, Germany). Remaining acetone was removed by rinsing with filtrated deionized water produced by a MilliQ apparatus (Millipore, Molsheim, France). Only under these conditions could contamination with dust be omitted. The sample volume was typically 200 μL. Polymerization was then started by addition of 40 μL imidazole, 30 mM, pH 7.0 (Fluka, Deisenhofen, Germany) and the appropriate amount of magnesium chloride. This solution was filtrated as well. In most experiments, a final concentration of 2 mM was used. Alternatively, 150 mM NaCl was used as polymerizing agent. Protein concentrations were determined by the method of Bradford (1976) calibrated by bovine serum albumin. Tests showed no detectable loss of protein during filtration. The samples were polymerized for 16 h in sealed cuvettes at room temperature (about 20°C).

Each sample was examined after the light scattering measurements by transmission electron microscopy. Negative staining was used for contrasting (Hayat and Miller, 1990). Fifteen microliters desmin solution were adsorbed for one minute onto glow-discharged, carbon-coated copper grids (Agar G2730C, 400 mesh, thin bar, Plano, Wetzlar, Germany). The grids were then washed twice with distilled water, stained for 1 min with uranylacetate (1% solution, Merck), and dried. Electron micrographs were taken the same day on Agfa ScientiaEM films (Agfa-Gevaert, Belgium) using a CM100 transmission electron microscope from Philips (Eindhoven, The Netherlands) operated at 100-kV acceleration voltage.

Dynamic light scattering

We used a light scattering spectrometer manufactured by ALV (Laservertriebsgesellschaft, Langen, Germany). It consisted of a mechanical goniometer setup (ALV-SP/125), a single photon detection unit (ALV SO-SIPD), and a digital multiple τ correlator system (ALV 5000/E, ALV 800, and ALV 5000/Fast). The light source was an argon ion laser (Innova

70–4, Coherent, Dieburg, Germany) operated at 488 nm. The sample cuvettes were housed in a thermostated index-matching bath (ALV) filled with toluene. The samples were kept at 10°C for at least half an hour before the first measurement and during the measurements. The scattering volume was approximately 0.1 mm^3 at a scattering angle of 90°. The alignment of the spectrometer was repeatedly checked by measuring the static scattering of toluene and water. Scattering angles ranging from 30° to 140° could be used, i.e., in this range of angles, the scattering intensities of these two low molecular-weight fluids showed less than 1% deviation from the expected $1/\sin\Theta$ dependence (Chu, 1991). Scattered light was collected by fiber optics (ALV), ensuring intercepts very close to two. In the photon detection unit, the incoming light was split and detected by two independent photomultipliers. The cross-correlation of both muliplier signals was measured. This allowed determination of the dynamic structure factor in a time window from 12.5 nsec to many seconds. Due to slight data distortions at the smallest correlation times, only data at correlation times exceeding 100 nsec could be used for evaluation. To test the performance of our setup, we also performed dynamic light scattering experiments on lysozyme, an extremely well characterized protein. For these experiments, lysozyme (Sigma) was dissolved at a concentration of 25 mg/mL in 50 mM sodium acetate buffer, filtrated through a 0.1-μm pore size filter (Nuclepore, Costar, Cambridge, MA.), and measured at 20°C at three different scattering angles (40°, 90°, 130°). At all scattering angles, the data could be well described by a cumulant fit (Pusey, 1974),

$$\ln(g^{(2)}(\tau) - 1) = -A_0 - \bar{\Gamma}\tau + \mu_2\tau^2 + \cdots, \qquad (9)$$

where A_0 is related to the intercept, $\bar{\Gamma}$ is the average decay rate, and μ_2 is the second cumulant. The z-average of the normalized variance of the distribution of the scatterer's diffusivity is given by $2\mu_2/\bar{\Gamma}^2$. We found a diffusion constant of 76 $\mu m^2/s$ and a polydispersity of 3–6%. These results coincide within the experimental error values in the literature (Muschol and Rosenberger, 1995). Neither by the Contin algorithm (Chu, 1991) nor by fitting to a biexponential law,

$$g^{(2)}(\tau) - 1 = [a_1\exp(-t/\tau_1) + a_2\exp(-t/\tau_2)]^2, \quad (10)$$

could we find any contributions at half the average decay rate $\bar{\Gamma}$. Therefore, no spurious heterodyning signal was present in our data. For heterodyning to occur, a local oscillator (e.g., a static reflex) is necessary (Chu, 1991). The static scattering of pure water clearly showed that no such reflex was present in this angular range. In polymer gels, heterodyning frequently occurs because of stationary inhomogeneities of the samples (Geissler, 1993). Because the desmin samples did not gel (see below in the Results section), it is highly unlikely that any inhomogeneities should have been stationary on the time scale of the duration of the measurements (30 min). Alternatively, light scattered from dust particles might act as local oscillator (Cummins and Pusey, 1977). Therefore, our samples were rigorously filtered. Measurements where dust crossed the scattering volume were discarded. If this happened more than once or twice with one sample, the whole sample was discarded. This strict procedure ensured data that were free of spurious heterodyning and background drift. In our experiments on lysozyme and on desmin, the baseline of the intensity correlation functions showed not more deviations from one than $2 \cdot 10^{-4}$. This value was determined by laser power fluctuations of about 1% with a correlation time of 10–100 s. This extremely low amount of baseline drift did not influence our results. Measurements where dust crossed the scattering volume exhibited a significantly larger background drift and yielded unreliable results in the data evaluation. This is another reason why the samples had to be free of dust. As a positive side effect, our clarification procedure resulted in sterile samples that could be used for a long time (see below). Geissler (1993) states that an intercept (i.e., the short time limes of $g^{(2)}$) close to two is a good indicator for pure homodyne operation of the instrument. Such high values of the intercept were achieved in all experiments on desmin and lysoyzyme. The laser power was adjusted to achieve count rates of approximately 100 kHz. The scattering intensity of polymerized desmin samples was approximately 140 times larger than the scattering from pure toluene. Because the Rayleigh ratio of toluene is well known (Chu, 1991), this comparison yields an estimate of 20 cm for the mean distance traveled by 488 nm light between successive scattering events. This distance is large compared to both the size of the scattering volume (largest dimension 1 mm) and the inner diameter of the cuvettes (8 mm). Therefore, multiple scattering played no role in our experiments. To ensure good statistics, we measured for 30 min at each scattering angle. For data modeling, the theoretical expressions for the field correlation function $g^{(1)}$ were converted into expressions for the intensity correlation function $g^{(2)}$ with the help of the Siegert relation, Eq. 1. Nonlinear least square fits of the model functions were performed by the Levenberg–Marquardt algorithm on a Macintosh PC using the software package Igor 3.0 (Wavemetrics, Lake Oswego, OR). The statistical errors of the experimentally determined correlation function were supplied by the spectrometer software (ALV; described in detail by Peters, 1993) and were used for correct weighting in the least square function χ^2. The quality of the fit results was judged by the resulting χ^2 value, the shape of the residual function $R(t)$, and the stability of the fit results against changes of the time window in which the fit was performed. The residual function $R(t)$ is defined as the difference between measured and fitted value normalized by the standard deviation of the measured value. Examples of measured data, fit results, and residual functions will be presented in the following section. To ensure reproducibility, the first measurement of a series was repeated at the end, and each series of measurements was repeated at least once.

RESULTS

Polymerization and aging of samples

Electron microscopy showed that homogeneous networks and polymer lengths of several micrometers could be achieved at Mg^{2+} concentrations of 2 mM and desmin concentrations in the range of 0.3 to 1.0 mg/mL. Polymers of insufficient length and inhomogeneous networks formed at desmin concentrations below 0.3 mg/mL. These samples could not be used for light scattering experiments. An electron micrograph of a typical network is displayed in Fig. 1. Please note that some of the preparation steps for negative staining introduce preferential orientation of the filaments.

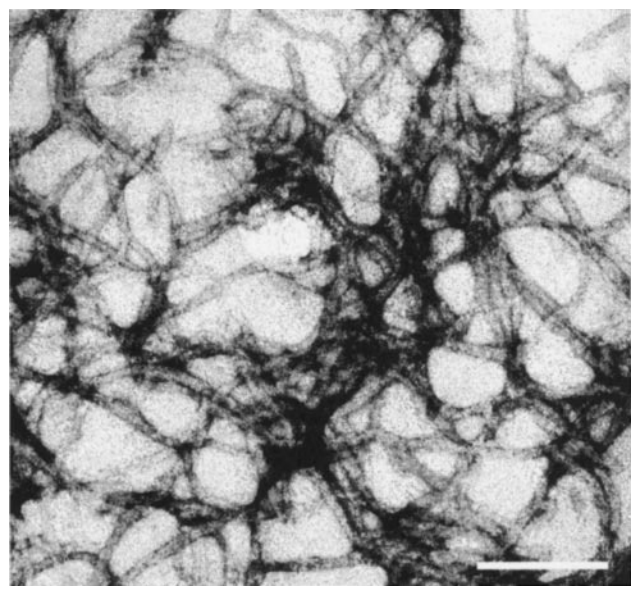

FIGURE 1 Electron micrograph (negative staining) of a representative desmin network. Experimental conditions were: 0.6 mg/mL desmin and 2 mM Mg^{2+}. Scale bar, 200 nm.

Therefore, it is very difficult to draw conclusions about the flexibility of the filaments from electron micrographs like Fig. 1. Some samples were prepared using 150 mM NaCl and a desmin concentration of 0.3 mg/mL. Again, homogeneous networks consisting of polymers of many-micrometer length were formed.

The results of light scattering measurements at short times after the beginning of polymerization could not be evaluated. We had to wait several hours after starting the polymerization before reproducible results could be achieved. This contrasts with the results of Herrmann et al. (1996) who used viscosimetry to monitor the assembly of vimentin filaments and found complete polymerization within half an hour after the polymerization started. The difference in time scale can be understood as follows. First, desmin and vimentin polymerization kinetics might differ. Second, we polymerized our samples at room temperature, whereas Herrmann et al. used physiological temperatures. Third, a small fraction of soluble units (tetra- or octamers) will remain undetected in viscosimetry. However, such soluble units would strongly disturb light scattering experiments because their length is about 65 nm in the case of vimentin (Herrmann et al., 1996). Particles of this size are efficient scatterers of light. Free diffusion of rods of this length leads to a decay of the intensity correlation function on about the same time scale as the observed dynamics of filaments. Therefore, contributions due to scattering by soluble units must be avoided in quasi-elastic light scattering experiments and our samples had to be very well equilibrated to minimize the concentration of such soluble material. For these reasons, samples were used at earliest 16 h after the polymerization was started. After this maturation period, an extremely low fraction of the overall protein mass was contained in short filaments. This was tested by electron microscopy of samples after maturation periods of 5 min and 16 h, respectively. Immediately after the induction of polymerization, most filaments had a length of less than 200 nm. After 16 h, such short filaments were rarely found in electron micrographs. Moreover, we centrifuged a sample after a maturation period of 16 h at 110,000 $\times$ g for 2 h. Electron micrographs of the supernatant showed very few filaments as compared to the resuspended pellet or samples that had not been centrifuged. The filaments in the supernatant exhibited lengths below 400 nm. Because electron microscopy is not well suited to determine protein densities, we used the protein assay of Bradford (1976) instead. The protein concentration in the supernatant was below the detection limit of this assay, which amounted to 2% of the total protein content in the sample before centrifugation. Therefore, we could safely neglect contributions from such short filaments in the data interpretation. The fact that no reproducible results could be achieved during the first 16 h of maturation most likely resulted from a variability of the maturation kinetics because of variances of temperature and concentration, as well as batch-to-batch variations of the protein itself. During maturation, the scattering intensity increased only weakly ($\sim$10%), which is not surprising because the filaments exhibited a length on the order of the wavelength of light already after 5 min, that is before they were inserted into the light scattering spectrometer.

Upon tilting the cuvettes, mature samples flowed slowly, albeit did not show any indications for gelation. The absence of gelation was necessary for our study because gelation frequently leads to parasitic heterodyning and nonergodicity, i.e., dynamic light scattering experiments at different locations in the sample yield different results (Geissler, 1993). In our experiments, we found that the decay of the dynamic structure factor was highly reproducible with respect to location in one sample and between different samples. Moreover, the scattering intensities showed no systematic fluctuations, and intercepts of the dynamic structure factor close to two were found. All these observations indicate that our samples were homogeneous and fluid on the time scale of the experiments, i.e., they did not form a gel. Additionally, we found no indications for cluster formation in electron micrographs.

Irradiating one scattering volume for 1 h with four times higher laser power than used in the normal experiments showed no significant change in the dynamic structure factor. Neither were the results changed by moving the cuvette to observe a region that was not previously exposed to light. From these two observations, we concluded that photochemical reactions due to the intense laser beam did not influence our results. Samples could be used up to three days before degradation took place, which was indicated by marked changes in the dynamic structure factor, see Fig. 2. Moreover, electron micrographs of such old networks could be clearly distinguished from pictures of freshly prepared networks. Significantly shorter and a high percentage of partially unraveled filaments were observed for old networks.

Initial decay

From all theoretical models, we expect a decay of the intensity correlation function that is single exponential at

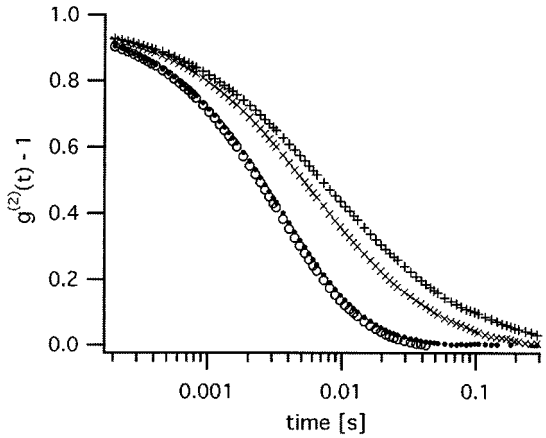

FIGURE 2 Aging of desmin networks. Shown is the decay of the intensity correlation function of a sample of 1.0 mg/mL desmin polymerized by 2 mM Mg^{2+} at 24 h (○), 42 h (●), 92 h (×) and 146 h (+) after start of the polymerization.

short times (initial decay) and, at larger correlation times, crosses over to a stretched exponential. We evaluated the initial decay by two different methods. First of all, we fitted the data at short times by a single exponential. The long time limit of the fit interval was varied and the quality of the fit was judged by χ^2, the shape of the residual function, and the variation of the fit results with changing limits of fit range. In most cases, good results were achieved (i.e., stable initial decay rates and no systematic variation of the residuals). An example for the quality of fit is shown in Fig. 3. Alternatively, we used cumulant fits of first and second order, see Eq. 3, varied the fit interval, and extrapolated the resulting values to correlation time 0. Typical results are shown in Fig. 4. For the first-order cumulant fit, the results of this procedure coincided with the results of single exponential fitting within the statistical uncertainty. For a second-order cumulant fit, the situation was more complex. At short correlation times, where the data could be well fitted by a single exponential, a second-order cumulant fit yielded results of extremely low statistical significance, that is, the data were overfitted. At larger correlation times, the resulting normalized second cumulants, $\mu_2/\bar{\Gamma}^2$ were very large (up to 10) and exhibited a significant variation with the interval used for data fitting. In other words, a second-order cumulant fit did not describe the data adequately in any interval. This failure had to be expected because the cumulant expansion is an analytical expansion of the logarithm of the correlation function around time 0. This procedure is adequate in samples exhibiting some polydispersity (e.g., lysozyme, see above), but, in our case, we expect a crossover from single exponential to stretched exponential decay ($\exp(-at^{\gamma})$; $0 < \gamma < 1$). Because the logarithm of a stretched exponential cannot be expanded around time 0, the cumulant expansion of order ≥ 2 cannot be applied to this problem.

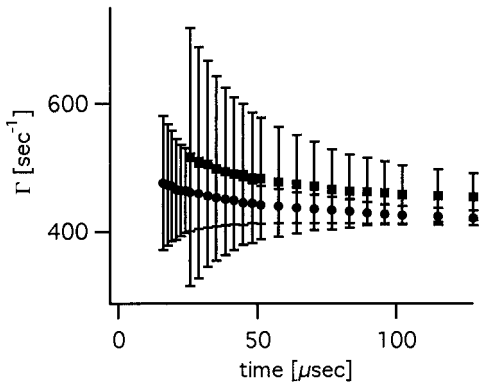

FIGURE 4 Initial decay rate, Γ, as determined by cumulant fits of first order (*circles*) and second order (*squares*) as function of the upper limit of the fit interval. The same experimental data were used as in Fig. 3. The error bars denote the statistical variance of the fit parameters as supplied by the Levenberg–Marquardt algorithm. Extrapolation to time 0 yielded $\Gamma = 480 \pm 40\ s^{-1}$ for the first-order cumulant fit. The low statistical significance of the fit results for the second-order cumulant fit rendered the same extrapolation meaningless in this case.

Within the Zimm model, the initial decay rate should scale with the third power of q (Dubois-Violette and de Gennes, 1967). However, including the semiflexible nature of the polymer in the theory results in a logarithmic correction to this scaling (Kroy and Frey, 1996). Therefore, examination of the initial decay rate allows discrimination between the two models. Figure 5 clearly shows that the initial decay rate Γ_i does not scale properly with q^3, but can be well described by the theory for semiflexible polymers. Moreover, all theoretical approaches within the Zimm model predict substantially faster decays than measured, see Fig. 5. Please note that we displayed the lowest result of all theoretical treatments within the Zimm model in Fig. 5 (see Eq. 4 and the paragraph following it). In this specific measurement, we measured a hydrodynamic diameter of

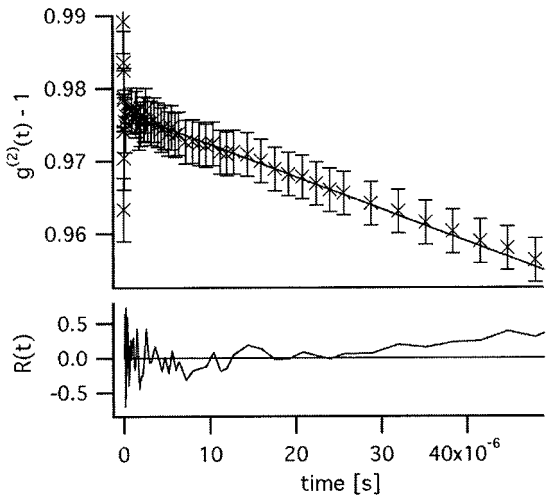

FIGURE 3 The initial decay of the intensity correlation function $g^{(2)}(t)$ fitted by a single exponential. Sample was 0.6 mg/mL desmin polymerized by 2 mM Mg^{2+} measured at a scattering angle of 40°. A single exponential function could be fitted to the data in a time window ranging from 100 nsec to 30 μsec. The initial decay rate was $460 \pm 60\ s^{-1}$.

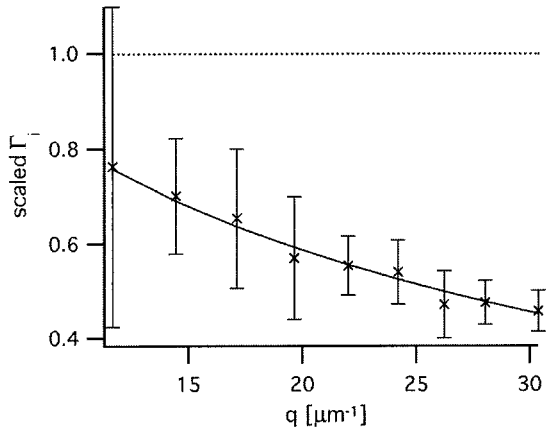

FIGURE 5 The normalized initial decay rate for a typical measurement. Displayed are the measured data (×), the Zimm prediction, Eq. 4, (*dotted line*) and the model function for a semiflexible polymer, Eqs. 5 and 6, with a thickness of 18 nm (*solid line*). For normalization, the data were divided by $3\ \pi\eta_s/(k_{BT}q^3)$.

18 ± 1 nm assuming no hydrodynamic screening (Eq. 6) and 17 ± 1 nm including screening (Eq. 7). The small difference between these results shows that hydrodynamic interactions were not important in our experiments. Initial decay measurements were performed at desmin concentrations of 0.4, 0.6, and 1.0 mg/mL for samples that were polymerized by 2 mM Mg^{2+} and at a desmin concentration of 0.3 mg/mL where polymerization was induced by 150 mM Na^{+}. No dependence of the hydrodynamic diameter a_h on the concentration or the salt conditions was found. The mean of all resulting values for a_h was 18 ± 2 nm assuming no hydrodynamic screening (Eq. 6), and 16 ± 2 nm including the screening effect (Eq. 7).

Long time decay of the correlation function

At longer times, the decay of the intensity correlation function cannot be described by a single exponential function. Examples for data measured at the same sample but different scattering angles are displayed in Fig. 6.

We tried to fit the data by different expressions, namely single exponential, a squared sum of two exponentials (Eq. 10), and a stretched exponential with exponent ¾ (see Eq. 8). For one specific measurement, the results are shown in Fig. 7. Obviously, the single and stretched exponential fit are not acceptable. The decay rates determined for the squared sum of two exponentials depended strongly on the interval chosen for the fit. Therefore, this fit is meaningless as well. The same holds for a stretched exponential fit where the exponent was adjusted, because the results for the exponent depended strongly on the fit interval. In Fig. 7, data are shown for a scattering angle of 40°. At larger scattering angles, the results were even worse because the fit interval had to be narrowed substantially to achieve the same quality of fit. For example, at 40° the fit interval ranged from 0.2 to 14.7 msec, whereas at 130° we had to select an interval ranging only from 0.5 to 8 msec to keep χ^2 for the stretched

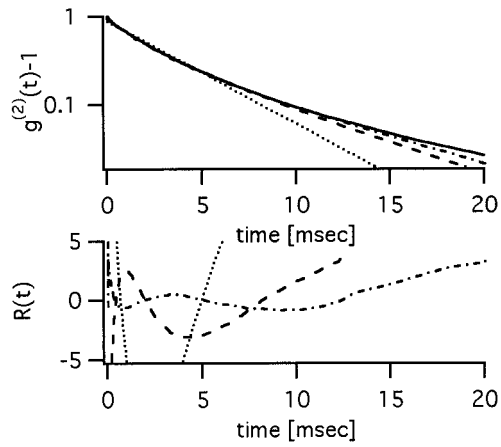

FIGURE 7 Long time decay of the intensity correlation function. Sample was 0.6 mg/mL desmin polymerized by 2 mM Mg^{2+}. Scattering angle was 40°. Data (*solid line*) were fitted using a single exponential (*dotted line*), a stretched exponential with exponent ¾ (*dashed line*), and a squared sum of two exponentials (*dash-dot line*). The fit interval ranged from 0.2 to 14.7 msec and was chosen so that the biexponential fit yielded an acceptable χ^2. Shown are fit functions (*top*) and the corresponding residuals (*bottom*).

exponential comparable. This is contrary to expectation, because, with increasing scattering vector, the product of scattering vector and persistence length increases and the model of a weakly bending rod should be better realized. Plotting $\ln(-\ln(g^{(2)} - 1))$ versus $\ln t$ showed that there is no obvious time window where the data might be modeled by a stretched exponential decay. Such a plot is also called a Kohlrausch plot.

In contrast, the correlation functions exhibit a characteristic frequency. This can be clearly seen when the data are plotted versus the dimensionless variable $x = \Gamma_i \times$ time. The initial decay rate Γ_i was determined as described above. An example for such a scaled plot is shown in Fig. 8. The data collapse nicely onto a universal curve that is a scaling function. Such a behavior is not expected for weakly bending rods unless $ql_p \rightarrow 1$. In this limit, the weakly bending

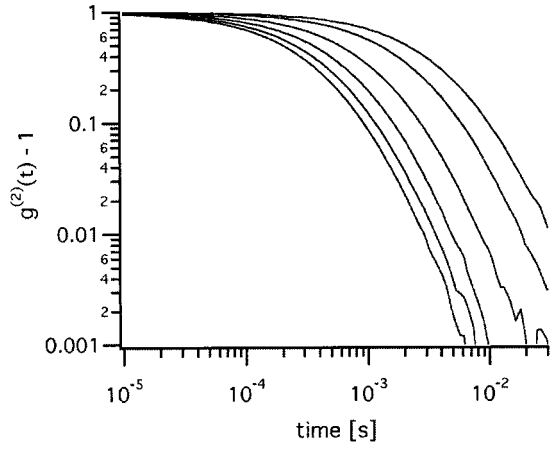

FIGURE 6 Intensity correlation functions $g^{(2)}$ measured at scattering angles of 40°, 50°, 70°, 90°, 110°, and 130° (from *right* to *left*). Sample was 0.6 mg/mL desmin polymerized by 2 mM Mg^{2+}.

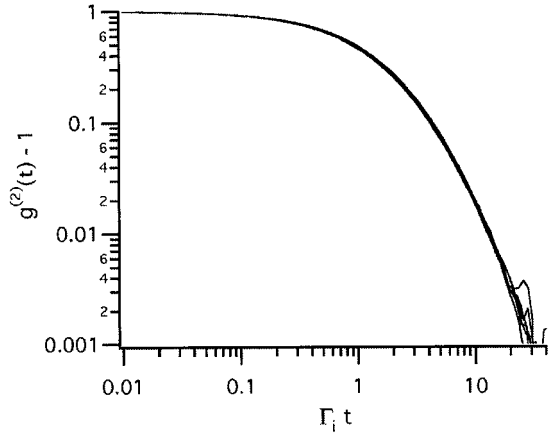

FIGURE 8 Same data as presented in Fig. 6, but each correlation function was plotted versus initial decay rate multiplied by time.

rod model cannot be considered quantitative, but one recovers the existence of one single characteristic frequency as in the case of the Rouse and Zimm models (Akcasu et al., 1980; see also the discussion at the end of the Theoretical Considerations section). In our experiments, the scaling function depends on the concentration of the polymer and the salt conditions, see Fig. 9. This had to be expected because the mesh size of the polymer network is not very much larger than the scattering length, and, therefore, some influence of the surroundings on the dynamics of a test polymer is likely. The influence of the salt conditions on the scaling function could arise because of possible salt-induced changes in the structure of the polymer itself (e.g., changes of the persistence length).

DISCUSSION

From a physics point of view, our findings are quite surprising. In the short time domain, the data are successfully described by a model that is based on the hydrodynamics of predominantly straight rods. The long time decay, however, lacks the scaling behavior characteristic of weakly bending rods. In other words, the existence of a characteristic frequency for the entire correlation function shows that flexing modes do not play any role, and the separation of time scales, as assumed in the theory for the dynamics of semiflexible polymers, has broken down. The latter fact gives an upper limit for the persistence length of approximately one micrometer. A stiffer polymer should clearly exhibit the stretched exponential decay characteristic for a semiflexible polymer. Up to now, the cross-over from weakly bending rod to fully flexible polymer was not described. Therefore, we cannot give a rigorous estimate for the lower limit of the persistence length below which the theory of Kroy and Frey (1996) for the initial decay breaks down. We estimate this lower limit to be about 0.1 μm. From this, it appears that the persistence length of desmin is on the order of 0.1–1 μm. A larger persistence length would lead to a stretched exponential tail of the correlation function, a shorter persistence length could presumably not be modeled by a predominantly straight rod.

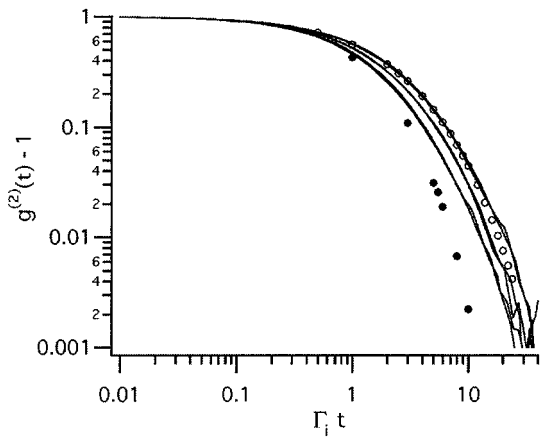

FIGURE 9 Representative measurements plotted versus normalized time for different conditions. These are 0.6 mg/mL and 1.0 mg/mL desmin concentration polymerized with 2 mM magnesium chloride and 0.3 mg/mL desmin polymerized with 150 mM sodium chloride (*full curves from left to right*). In each case, the measured data at scattering angles of 40° and 90° are shown. Additionally the scaling functions of the Rouse (*open circles*) and the Zimm (*full circles*) models are displayed. These were taken from Akcasu et al. (1980).

The fact that the data exhibit a characteristic frequency is remarkable, because it indicates that flexure modes of the filaments are irrelevant for the dynamic structure factor, and only diffusion of internal modes of polymer dynamics are observed. This is the same situation as in the Rouse and Zimm models. However, in our case, neither model fits the data. This can be seen because there is no possibility to fit the initial decay rate by either model (see Fig. 5). Moreover, the form of the scaling function is close to the scaling functions of the Zimm and Rouse models if we use the measured initial decay rate instead of the characteristic frequency predicted by both models; yet there are marked deviations. This is reasonable because 1) it is impossible to model the hydrodynamic interactions between continuous polymers of finite thickness (thread-like or rod-like polymers) by a bead spring model, and 2) the mesh size of the networks is not extremely larger than the scattering length, therefore concentration effects on the scaling function are expected (and were indeed observed). This latter effect is not included in any asymptotic theory.

The remarkable flexibility of desmin filaments is surprising. For an isotropic rod, the bending rigidity scales with the fourth power of the diameter, yet actin filaments are at least ten times stiffer (Ott et al., 1993; Gittes et al., 1993; Käs et al., 1994) than desmin filaments while having a substantially smaller diameter (Steven et al., 1982; Sheterline et al., 1995). Therefore, it appears that desmin filaments are either composed of an extremely flexible material or that there are certain localized weak spots in the structure. The last alternative seems more probable because the structure of type III IFs is not as well defined as for other biopolymers (Heins and Aebi, 1994). Additionally, the radial density profile of dry material in IFs was measured and found to be 0.5 g/cm^{-3} and less (Steven, 1990). On the basis of both findings, the only loosely defined architecture, and the low protein density in type III IFs, the existence of defects in the filament architecture seems likely. It is possible that the observed polymer dynamics is not due to bending of a continuous rod as assumed in the Kratky–Porod model (Kratky and Porod, 1949). A filament consisting of stiff, short rods connected by joints might describe the situation better. Another alternative would be that the building blocks of the filament adhere only weakly like the threads in a loosely twisted rope.

Extremely little is known about the conformations of head and tail domains of type III IF proteins (Parry and Steinert, 1995). However, a number of functions were attributed to these domains. These include diameter control during polymerization (Herrmann et al., 1996), and binding to membranes (Georgatos et al., 1987) and to DNA (Vorgias

and Traub, 1986). Moreover, phosphorylation sites are contained in the head domain of desmin whose state of phosphorylation may be used for assembly control of desmin in living cells (Geisler and Weber, 1988). We found a hydrodynamic diameter of desmin filaments of 16–18 nm, exceeding the standard value of 12 nm that is seen in electron microscopy using negative staining. The radial density profiles of dry material were determined by scanning transmission electron microscopy of freeze-dried IFs (Steven et al., 1982; Steven, 1990). These data show a central dense zone of about 10-nm diameter surrounded by a 2–3-nm-thick corona of reduced density. Our finding of a hydrodynamic diameter of 16–18 nm for native desmin filaments in buffer is in full accord with these results from electron microscopy. It seems highly likely that the head and tail domains of desmin contribute significantly to this loose layer (Steven, 1990) and are thus accessible for modifying enzymes and binding partners. Therefore, the model of a loose corona surrounding the dense IF core is in accordance with putative biological functions of desmin. However, the interpretation of these measurements is complicated by the fact that both mass per length and diameter of type III IFs exhibit a certain variability among different filaments and along the length of a single filament (Heins and Aebi, 1994). Recently, it was found that desmin and vimentin differ significantly in their mass per length ratio, although they are both type III IFs (Herrmann et al., 1997). This indicates that IFs are more heterogeneous than previously assumed. The question arises whether the core–shell model proposed by Steven is applicable to all IFs, and whether there is a correlation between protein sequence and the thickness of the loose surface layer.

However, there are many more open questions. The role of the structural variants (i.e., filaments with different thicknesses in one sample, and even thickness variations along a single filament's contour) and the existence of packing defects are to be explored. Of paramount importance remains the question of how the unusual mechanical properties of IFs come to be.

We thank Erich Sackmann for steady support and many helpful discussions. Roman Götter helped in the initial phase of the project. We thank Drs. Weber (Göttingen) and Herrmann (Heidelberg) for helpful hints and discussions on the protein preparation, Prof. Schmidt and Dr. Fischer (Mainz) for their advice on laser light scattering, and Dr. Michael Bärmann for his assistance in protein preparation and careful reading of the manuscript. This work was funded by the Deutsche Forschungsgemeinschaft via Sonderforschungsbereich 266.

REFERENCES

Akcasu, A. Z., M. Benmouna, and C. C. Han. 1980. Interpretation of dynamic scattering from polymer solutions. *Polymer* 21:866–894.

Alberts, B., D. Bray, J. Lewis, M. Raff, K. Roberts, and J. Watson. 1994. Molecular Biology of the Cell, 3rd ed. Garland, New York. 787–861.

Arcovito, G., F. A. Bassi, M. De Spirito, E. Di Stasio, and M. Sabetta. 1997. Dynamic light scattering study of fine semiflexible fibrin networks. *Biophys. Chem.* 67:287–292.

Benmouna, M., and A. Z. Akcasu. 1980. The effect of preaveraging the Oseen tensor on the characteristic frequency in good solvents. *Macromolecules*. 13:409–414.

Berne, B. J., and R. Pecora. 1976. Dynamic Light Scattering. John Wiley and Sons, New York.

Bradford, M. 1976. A rapid and sensitive method for the quantization of microgram quantities of protein utilizing the principle of protein-dye binding. *Analyt. Chem.* 72:248–254.

Chou, R.-G. R., M. H. Stromer, R. M. Robson, and T. W. Huiatt. 1990. Determination of the critical concentration required for desmin assembly. *Biochem. J.* 272:139–145.

Chu, B. 1991. Laser Light Scattering: Basic Principles and Practice, 2nd ed. Academic Press, San Diego.

Cummins, H. Z., and P. N. Pusey. 1977. Dynamics of macromolecular motion. *In* Photon Correlation Spectroscopy and Velocimetry. H. Z. Cummins, E. R. Pike, editors. Plenum Press, New York. 164–199.

de Gennes, P.-G. 1967. Quasi-elastic scattering of neutrons by dilute polymer solutions. I. Free-draining limit. *Physics*. 3:37–45.

Doi, M., and S. F. Edwards. 1986. The Theory of Polymer Dynamics. Oxford University Press, Oxford, U.K.

Drögemeier, J., H. Hinssen, and W. Eimer. 1994. Flexibility of F-actin in aqueous solution: a study on filaments of different average lengths. *Macromolecules*. 27:87–95.

Dubois-Violette E., and P.-G. de Gennes. 1967. Quasi-elastic scattering by dilute, ideal polymer solutions. II. Effects of hydrodynamic interactions. *Physics*. 3:181–198.

Edwards, S. F., and M. Muthukumar. 1984. Brownian dynamics of polymer solutions. *Macromolecules.* 17:586–596.

Farge, E., and A. C. Maggs. 1993. Dynamic light scattering from semiflexible polymers. *Macromolecules*. 26:5041–5044.

Fuchs, E., and K. Weber. 1994. Intermediate filaments: structure, dynamics, function and disease. *Annu. Rev. Biochem.* 63:345–382.

Fujime, S., S. Ishiwata, and T. Maeda. 1984. Dynamic light scattering study of muscle F-actin. *Biophys. Chem.* 20:1–21.

Geisler, N., and K. Weber. 1980. Purification of smooth-muscle desmin and a protein-chemical comparison of desmins from chicken gizzard and hog stomach. *Eur. J. Biochem.* 111:425–433.

Geisler, N., and K. Weber. 1988. Phosphorylation of desmin in vitro inhibits formation of intermediate filaments: identification of three kinase A sites in the aminoterminal head domain. *EMBO J.* 7:15–20.

Geissler, E. 1993. Dynamic light scattering from polymer gels. *In* Dynamic Light Scattering. The Method and Some Applications. W. Brown, editor. Clarendon Press, Oxford, U.K. 469–511.

Georgatos, S. D., K. Weber, N. Geisler, and G. Blobel. 1987. Binding of two desmin derivatives to the plasma membrane and the nuclear envelope of avian erythrocytes: evidence for a conserved site-specificity in intermediate filament-membrane interactions. *Proc. Natl. Acad. Sci. USA*. 84:6780–6784.

Gittes, F., B. Mickey, J. Nettleton, and J. Howard. 1993. Flexural rigidity of microtubules and actin filaments measured from thermal fluctuations in shape. *J. Cell Biol.* 129:923–934.

Goldman, R. D., R. V. Zackroff, and P. M. Steinert. 1990. Intermediate filaments—an overview. *In* Cellular and Molecular Biology of Intermediate Filaments. R. D. Goldman and P. M. Steinert, editors. Plenum Press, New York. 3–17.

Götter, R., K. Kroy, E. Frey, M. Bärmann, and E. Sackmann. 1996. Dynamic light scattering from semidilute actin solutions: a study of hydrodynamic screening, filament bending stiffness, and the effect of tropomyosin/troponin-binding. *Macromolecules*. 29:30–36.

Harnau, L., R. G. Winkler, and P. Reineker. 1995. Dynamic properties of molecular chains with variable stiffness. *J. Chem. Phys*. 101: 7750–7757.

Hayat, M. A., and S. E. Miller. 1990. Negative Staining. McGraw-Hill, New York.

Heins, S., and U. Aebi. 1994. Making heads and tails of intermediate filament assembly, dynamics and networks. *Curr. Op. Cell Biol.* 5:25–33.

Herrmann, H., and U. Aebi. 1998. Intermediate filament assembly: fibrillogenesis is driven by decisive dimer–dimer interactions. *Curr. Op. Struct. Biol.* 8:177–185.

Herrmann, H., M. Häner, M. Brettel, and U. Aebi. 1997. Distinct early assembly units of different intermediate filament proteins. *Mol. Biol. Cell.* 8:392a.

Herrmann, H., M. Häner, M. Brettel, S. A. Müller, K. N. Goldie, B. Fedtke, A. Lustig, W. W. Franke, and U. Aebi. 1996. Structure and assembly properties of the intermediate filament protein vimentin: the role of its head, rod and tail domains. *J. Mol. Biol.* 264:933–953.

Houseweart, M. K., and D. W. Cleveland. 1998. Intermediate filaments and their associated proteins: multiple dynamic personalities. *Curr. Op. Cell Biol.* 10:93–101.

Huiatt, T. W., R. M. Robson, N. Arakawa, and M. Stromer. 1980. Desmin from avian smooth muscle. Purification and partial characterization. *J. Biol. Chem.* 255:6981–6989.

Inagaki, M., Y. Nishi, K. Nishizawa, M. Matsuyama, and C. Sato. 1987. Site-specific phosphorylation induces disassembly of vimentin filaments in vitro. *Nature*. 328:649–652.

Janmey, P. A., U. Euteneuer, P. Traub, and M. Schliwa. 1991. Viscoelastic properties of vimentin compared with other filamentous biopolymer networks. *J. Cell Biol.* 113:155–160.

Janmey, P. A., J. Peetermans, K. S. Zaner, T. P. Stossel, and T. Tanaka. 1986. Structure and mobility of actin filaments as measured by quasielastic light scattering, viscometry, and electron microscopy. *J. Biol. Chem.* 261:8357–8362.

Käs, J., H. Strey, and E. Sackmann. 1994. Direct imaging of reptation for semiflexible actin filaments. *Nature*. 368:226–229.

Kratky, O., and G. Porod. 1949. Röntgenuntersuchung gelöster Fadenmoleküle. *Recl. Trav. Chim. Pays-Bas.* 68:1106–1122.

Kroy, K., and E. Frey. 1996. Dynamic scattering from solutions of semiflexible polymers. *Phys. Rev. E* 55:3092–3101.

Kroy, K., and E. Frey. 1998. Dynamic scattering from semiflexible polymers. *In* Scattering in Polymeric and Colloidal Systems. W. Brown and K. Mortensen, editors. Gordon and Breach, New York. In press.

Lazarides, E. 1980. Intermediate filaments as mechanical integrators of cellular space. *Nature*. 283:249–256.

Maeda, T., and S. Fujime. 1984. Spectrum of light quasi-elastically scattered from solutions of semiflexible filaments in the dilute and semidilute regimes. *Macromolecules.* 17:2381–2391.

Maeda, T., and S. Fujime. 1985. Dynamic light scattering study of suspensions of fd virus. Application of a theory of light-scattering spectrum of weakly bending filaments. *Macromolecules*. 18:2430–2437; Erratum. 1986. *Macromolecules.* 19:1494.

Miller, R. K., K. Vistrom, and R. D. Goldman. 1991. Keratin incorporation into intermediate filament networks is a rapid process. *J. Cell Biol.* 113:843–855.

Milner, D. J., G. Weitzer, D. Tran, A. Bradley, and Y. Capetanaki. 1996. Disruption of muscle architecture and myocardial degeneration in mice lacking desmin. *J. Cell Biol.* 134:1255–1270.

Muschol, M., and F. Rosenberger. 1995. Interactions in undersaturated and supersaturated lysozyme solutions: Static and dynamic light scattering results. *J. Chem. Phys.* 103:10424–10432.

O'Connor, C. M., D. R. Balzer, and E. Lazarides. 1979. Phosphorylation of subunit proteins of intermediate filaments from chicken muscle and nonmuscle cells. *Proc. Natl. Acad. Sci. USA*. 76:819–823.

Ott, A., M. Magnasco, A. Simon, and A. Libchaber. 1993. Measurement of the persistence length of polymerized actin using fluorescence microscopy. *Phys. Rev. E.* 48:R1642–R1645.

Parry, D. A. D., and P. M. Steinert. 1995. Intermediate Filament Structure. Springer, New York.

Peters, R. 1993. Noise on photon correlation functions and its effect on data reduction algorithms. *In* Dynamic Light Scattering. The Method and Some Applications. W. Brown, editor. Clarendon Press, Oxford. 469–511.

Pusey, P. N. 1974. Macromolecular diffusion. *In* Photon Correlation and Light Beating Spectroscopy. H. Z. Cummins and E. R. Pike, editors. Plenum Press, New York. 387–428.

Quinlan, R., C. Hutchison, and B. Lane. 1995. Differentiation-related expression. *In* Protein Profile, Intermediate Filament Proteins, Vol. 2. P. Sheterline, editor. Academic Press, London. 809–814.

Sheterline, P., J. Clayton, and J. C. Sparrow. 1995. Actin structure. *In* Protein Profile, Actin, Vol. 2. P. Sheterline, editor. Academic Press, London. 14–46.

Small, J. V., D. O. Furst, and L.-E. Thornell. 1992. The cytoskeletal lattice of muscle cells. *Eur. J. Biochem.* 208:559–572.

Steven, A. C., J. Wall, J. Hainfield, and P. M. Steinert. 1982. Structure of fibroblastic intermediate filaments: analysis by scanning transmission electron microscopy. *Proc. Natl. Acad. Sci. USA*. 79:3101–3105.

Steven, A. C. 1990. Intermediate filament structure. Diversity, polymorphism, and analogy to myosin. *In* Cellular and Molecular Biology of Intermediate Filaments. R. D. Goldman and P. M. Steinert, editors. Plenum Press, New York. 233–263.

Stewart, M. 1990. Intermediate filaments: structure, assembly and molecular interactions. *Curr. Op. Cell Biol.* 2:91–100.

Vorgias, C. E., and P. Traub. 1986. Nucleic acid binding activities of the intermediate filament subunit proteins desmin and glial fibrillary acidic protein. *Z. Naturforsch.* 41C:897–909.

Zhou, H., T. W. Huiatt, R. M. Robson, S. W. Sernett, and D. J. Graves. 1996. Characterization of ADP-ribosylation sites on desmin and restoration of desmin intermediate filament assembly by de-ADP-ribosylation. *Arch. Biochem. Biophys.* 334:214–222.

Zimm, B. H. 1956. Dynamics of polymer molecules in dilute solution: viscoelasticity, flow birefringence and dielectric loss. *J. Chem. Phys.* 24:269–278.